ORIGINAL PAPER

D. Mukherjee · T.M. Balasubramanian
J. Mathiyarasu · Samrat Mukherjee

Innovative processing using ultrafine particulation

Abstract Anodic sites like grain-boundaries, micro-voids, micro-inclusions and other stress concentration points such as dislocations, vacancies, etc., take an active part in the galvanic interactions occurring on the surface of metals and alloys. This paper discusses the role of low concentration reinforcement of metals like Zn, Pb and Sn, alloy matrices like Cu-Zn, Cu-Mn, Zn-Al and Al-Zn and non-metals like polyaniline, along with the amorphous Ni-P-B class of current-assisted electroless deposits. It is assumed that ultrafine ceramic particulates in low concentration ranges (1–1.5 wt%) may cover the anodic defect sites such that these anodic boundaries start behaving cathodically as a network, within the already existing cathodic grain matrices, because they are predominantly more cathodic, compared to the grain boundaries, voids, etc. As such, there is a considerable reduction of surface dissolution and in the anodic current of the matrix. It has been shown that surface dissolution is a minimum for a critical threshold concentration of the particulates, above which there is drastic dissolution of the surface. It appears that particulates above that critical concentration cannot be accommodated within the available anodic sites, such that they are dispersed on the grain proper in a random fashion, creating stress spikes and subsequent enhanced matrix dissolution. It further appears that it will thus be possible either to decrease or increase the dissolution of the composite matrices for selective tailor-made applications, by changing the concentration of these ultrafine particulates around the threshold concentration. It has been shown that such a technique may eventually reduce the leaching of copper from conventional brass matrices and also reduce the dissolution of tin in the packaging industries. Grain boundary structures of the metallic matrices have also been correlated with the particulate trapping capacity and their corresponding galvanic stress factors. It has also been applied to amorphous Ni-P-B types of metal-metalloid coatings, for enhancement of surface corrosion resistance. Particulation of epoxy and epoxy-silicone classes of barrier with ultrafine SiC has revealed a more positive potential and lower galvanic currents. Reinforcement of the permalloy type Ni-Fe-Mo class barrier with fine Al_2O_3 particulates has indicated considerable improvement of the polarization resistance values.

Key words Ultrafine ceramic particulates · Matrix reinforcement · Grain boundary structure · Particulate trapping capacity · Galvanic stress factor

D. Mukherjee (✉) · T.M. Balasubramanian · J. Mathiyarasu
Central Electrochemical Research Institute,
Karaikudi-630 006, India

S. Mukherjee
U.D.C.T, Mumbai, India

Introduction

Anodic sites, like grain boundaries, voids, inclusions and other stress concentration points like dislocations, vacancies, etc., are the preferential sites for metallic corrosion to take place on the surface of metals and alloys [1–3]. Under such circumstances, incorporation of ultrafine ceramic particulates in a low concentration range in metals and alloys may be effective in the formation of a cathodic coverage on these anodic sites, such that the galvanic relationship between the anodic boundaries and other defects with the cathodic grain proper is somewhat moderated. There is then an effective reduction of the galvanically induced dissolution from the surface of the metals and alloys [1, 2].

However, conventional macroscopic powders normally induce stress raiser sites on the matrix and increase dissolution, although the surface hardness and the abbrasion resistance values are improved to a considerable extent. The probability of coverage of microscopic surface sites appears only when microscopic and preferably ultrafine particulates are incorporated in the matrix. As the total anodic sites of a matrix is limited, it further appears that there is a limit up to which the ultrafine

particulates may be accommodated on the matrix anodic sites. Above this limit, these particulates may eventually disperse in the grain proper and may also coagulate, forming stress raiser sites which enhance matrix dissolution. Thus the dissolution of a metallic surface may be made a function of the concentration of the ultrafine particulates incorporated in the matrix, such that dissolution may be either increased or decreased by altering the concentration of these particulates above or below this threshold critical limit. Such processing may, therefore, be useful in solving the compatibility related problems of composite structures like steel with brass and steel with alloys of zinc. The galvanic incompatibility of these systems may be considerably reduced by making the brass component more active and the zinc alloy more inert, compared with the adjoining steel structures.

De-alloying of brass is a well-known process [1], where one of the components, either copper or zinc, or both, may undergo leaching. Attempts have been made to resist such selective leaching, employing conventional surface modification techniques and using suitable inhibitors, but resulting in only marginal improvement of the resistance to dealloying. Incorporation of ultrafine ceramic particulates of matching galvanic activity, added in a low concentration range, may eventually improve the resistance to such de-alloying process. De-alloying is also observed in other bimetallic alloys, like Cu-Mn, Zn-Al, etc., where one component becomes more active than the other. This establishes a distinct galvanic strain on the matrix.

Such ultrafine particulation may also be applied on metallic matrices like pure zinc, lead, tin, aluminium and their alloys. Zinc and its alloys are popular coating materials, extensively employed in industry. Zinc also finds use in cathodic protection. Ultrafine particulation of zinc and its alloys for corrosion protection and those of tin and its alloys for food packaging are two emerging areas to be considered.

The authors in this paper discuss all these aspects, in the light of their probable roles in the improvement of surface properties. The behaviour of the copper-manganese group of promising marine alloys, and those of the nickel-based metal-metalloid type of barrier layers, are also discussed, highlighting the improvement of surface properties as a result of the low concentration reinforcement (1–1.5 wt%) of ultrafine particulates. Physicochemical properties of particulated Cu60-Zn40 brass and polyaniline matrices are also discussed. Some correlations have also been made between the grain structure and the concentration of ultrafine particulates, stressing their galvanic relationships.

State of art report

Advanced generation composites having a tensile strength of up to 600 MPa and a composite flexural strength of 4000 MPa has been achieved. The upper application temperature of carbon fibre is extremely high, varying from 1200 °C to 2000 °C. Recently, composite glasses and oxide matrices have been designed for use in an oxidizing environment, e.g. Nicalon, fibre reinforced glasses and other glass ceramics like lithium aluminium silicate. In these matrices the fracture strength of the fibres plays a very important role, as fracture will theoretically start in the fibres rather than the matrix. In the carbon carbon-fibre reinforced matrices, both the application temperature and the matrix strength are very high, where the total load is advantageously shared by both the carbon fibre and the carbon matrix in a more compatible mode.

These advanced composites lack adequate ductility and hence posses inadequate formability, in spite of the fact that cubic zirconium has some metallic properties. On the other hand, most of the metal matrix composites have comparatively superior ductility, as most of the metals are somewhat more ductile than the ceramics. As a first approximation, the total strength and ductility of a composite matrix may be computed by using the additive rule, considering the matrix and reinforcement separately. However, the brittleness function of such matrices appears to be a function of the misorientation of these particulates and also their effective concentration, much in excess of the residual ductility of the matrix. Obviously the matrix reliability and susceptibility to fatigue-type propagation will depend on the total effective brittleness, comprising stress concentration in the uniformly particulated zones and the localized stress spikes due to the segregation of particulates. On the other hand, the electrochemical properties of a composite matrix may be approximated, using a subtractive mode of potential computation within the galvanic domain of the matrix. The galvanic difference between the reinforcement and the matrix, in terms of potential, should be minimal for the lower chemical reactivity of the composite matrix. For such a computation, the more negative potential is subtracted from the more positive one.

A literature survey for the last 10 years did not reveal any systematic studies in the field of composite systems and particulate reinforcement for corrosion protection of metallic and non-metallic surfaces, except some references [4–12] on electroplated thin layers of Zn, Cr, etc., plasma nitriding and plasma coating processing of tin borides, intermetallics like Fe-Al, Ti-Al, etc., and metallic carbides, along with the nitrides of Ti and Zr. However, some corrosion studies, conducted on aluminium-silicon carbide composites [13], have revealed that SiC particulates behave as cathodic centres, creating localized low pH and enhanced corrosion. It should be borne in mind that SiC particulates used in these composite matrices are not of the ultrafine variety and the concentration of the particulates also exceeds the threshold low concentration range of 1–2% required for the deactivation of the anodic grain boundaries and other defect sites. As

such, most of these particulates are preferably dispersed in the grain proper in a random fashion, creating cathodic points and stress spikes which initiate galvanically induced leaching of the matrix, owing to their unique spatial location on the more anodic grain matrix (grain proper). Moreover, the very high susceptibility of Al with oxygen also creates oxide debris on the grain channels, and other anodic sites, making mismatches between the oxides, carbides and the matrix. The galvanically induced leaching of the matrix, owing to the cathodic nature of the reinforcing particulates, is a common menace for conventional metal-matrix composites. Therefore, an attempt has been made in this study to substitute the conventional particulates with the ultrafine variety and bring down the reinforcement concentration to a low range of 1–2% for reducing the galvanic activity of the metallic matrices.

Experimental

The pure metals, like Cu, Zn, Al, Mn, Pb and Sn, used in this study were of 99.9% purity. Ultrafine particulates, 1–2 μm of SiC, BC, WC, Al_2O_3 and TiO_2, used for preparing the composite matrices, were of A.R. grade. The glass powders used were of the borosilicate variety, of mesh size 250. Polyaniline, Fe-based metallic glass and steel powders were collected from the stocks of the laboratory. The steel powders used were of 800 mesh size. The Met-glass panels were obtained from Allied Chemicals. The nickel plating chemicals, used in obtaining particulated amorphous Ni-P-B on a MS substrate, were of analytical reagent quality. A conventional Ni-P bath was modified by using sodium borohydride as an additive. A current density equivalent to 150 A.S.F. was employed for accelerating deposition from the electroless bath. A standard (acid) $ZnCl_2^-$, based plating bath was employed for obtaining the Zn-Al_2O_3 composites. Deposition was conducted under potentiostatic control, employing mechanical stirring of the bath. The coarse Al_2O_3 powder used in the study was of 250 mesh size.

Bulk composite matrices were obtained by using the conventional routes of melting, thorough particulate mixing in the thixotropic state and casting. Preheating of the particulates was done for better matrix particulate wetting. The finer (0.01 mm^2) and coarse fractions (0.1 mm^2) of the metallic glass used in making the polyaniline matrix composites were obtained by mechanical means.

Electrochemical anodic and cathodic polarization and subsequent Tafel extrapolation techniques were used for obtaining the I_{corr}, B_a and B_c values, where the first one is the equivalent amount of corrosion current and the second and the third ones stand for the anodic Tafel slope and cathodic Tafel slope, respectively. Corrosion loss values based on mass loss have been expressed in terms of mg/dm^2/day (mdd) as per ASTM G31/71. A standard magnetic flux generating machine, made in the USA, has been employed for performing the mass-loss experiments in presence of a 150 G magnetic field. Standard potentiodyne equipment (made in the USA) was employed for obtaining the Tafel parameters, while a digital multimeter (made in the UK) was used for the measurement of open circuit potential values. All the electrochemical parameters (current and potential) reported in this study have been obtained with reference to the saturated calomel electrode (SCE). Dealloying experiments have been followed up by atomic absorption spectroscopy, available at the Central Electrochemcial Research Institute, Karaikudi. Photo-potential values have been recorded using a fabricated set-up recently organized in the spectroscopic wing of the Corrosion Science and Engineering laboratory. Hardness values have been recorded using a Rockwell machine and later converted to the Brinnel number (BHN). Other mechanical

parameters, like ultimate tensile strength (UTS) and percentage elongation values, have been obtained from the Instron facility of the Institute. Metallographic examination of the composite surfaces and the microstructures thereof were obtained by using optical microscopes [Reichard (made in Austria), Neophot 21 (made in Germany)] and a scanning electron microscope (SEM) [JEOL (made in Japan)] has been employed to study the grain boundary and particulate structures and their correlations, employing the conventional quantitative metallurgy route.

Results

Table 1 gives the hardness and I_{corr} values of the Cu60-Zn40 composite alloy matrix as a function of reinforcing phases like WC and BC. It is seen that compared to the unparticulated Cu-Zn matrix, the reinforced matrices reveal higher hardness values and lower I_{corr} values. Reinforcement of the matrix with 1% BC increases the hardness values and reduces the I_{corr} values to a minimum. These data clearly indicate that incorporation of ultrafine ceramic particulates in a low concentration range (1–1.5 wt%) improves the surface properties to a considerable extent in a neutral pH medium.

Table 2 gives the photopotential values of the Cu60-Zn40 composite alloy as a function of the type of reinforcement in 0.5 M NaOH electrolyte. The surfaces of the CuZn composite alloy have been exposed to a polychromatic mercury-xenon lamp for their electrical response, as light may be employed qualitatively to study the thickening of the film formed during immersion in an electrolyte. In all cases the potential differences measured are positive, indicating that the films are p-type semiconductive in nature [14]. It is noted that, compared to the unparticulated Cu60-Zn40 matrix, there is an increasing trend in the value of the photopotential in the more positive direction as a result of reinforcement with 1% WC, 1% SiC or 1% BC.

Table 1 Hardness (BHN) and I_{corr} (μA/cm^2) values of Cu60-Zn40 composite alloy, as a function of the type of reinforcement (particulate = ultrafine)

Matrix	Hardness	I_{corr} (μA/cm^2) (electrolyte = 3% NaCl)
Cu-Zn	376	0.0122
Cu-Zn + 1.0% WC	455	0.010
Cu-Zn + 1.0% BC	570	0.001

Table 2 Photopotential values of Cu60-Zn40 composite alloy, as a function of the type of reinforcement (light source: 250 W Hg-Xe, polychromatic; electrolyte = 0.5 M NaOH; particulate = ultrafine)

Matrix	Photo-potential (mV)		
	Instantaneous	After 1 h	After 4 h
Cu-Zn	+ 0.10	+ 0.5	+ 0.55
Cu-Zn + 1% WC	+ 0.10	+ 1.0	+ 1.78
Cu-Zn + 1% SiC	+ 0.12	+ 1.04	+ 1.95
Cu-Zn + 1% BC	+ 0.16	+ 1.05	+ 2.15

Looking at the data in the vertical and horizontal directions, it is further observed that the level of the positive potential and its shift is a maximum for the Cu-Zn-BC composite matrix. Assuming the increase in the value of the positive potential to be proportional to the thickness of the protective oxide scale, it can be inferred that particulation improves the film properties of the Cu-Zn system in the high pH medium.

Table 3 lists de-alloying data for the Cu60-Zn40-SiC composite alloy in a mixed electrolyte, comprising NaCl, $NaNO_2$ and Na_2SO_4 at room temperature. It is clear from the trend of the data that the de-alloying tendency becomes a minimum at around a SiC concentration of 0.3%. However, there appears to be an overall aggravation of matrix de-alloying, both above and below this concentration. Moreover, the overall de-alloying of zinc appears to be more than that of copper.

Table 4 shows the hardness (BHN) and I_{corr} (mA/cm^2) values of Cu70-Mn30 composite alloys as a function of the type of reinforcement. It is seen that reinforcement of a Cu-Mn bulk matrix with 1 wt% TiO_2, 1 wt% Al_2O_3 and 1 wt% SiC particulates results in the increasing improvement of surface hardness values, compared to those of the unreinforced matrices assuming the level of reinforcement of the bulk and of the surface to be more or less identical. A low concentration of reinforcement also reduces the I_{corr} values, which is more pronounced in the case of 1% TiO_2 and 1% Al_2O_3 particulates. It is seen that there is a drastic reduction of the mass-loss value, for a comparable thickness of the Cu-Mn barrier layer, as a result of particulation with ultrafine Al_2O_3.

Table 5 gives the thickness and electrochemical properties of a cerium-deoxidized Zn97-Al3 coated MS substrate, with and without SiC partciulation. It is seen that the SiC-reinforced matrix reveals a lower mass-loss value and more positive open circuit potential (OCP) at a comparable thickness of the zinc alloy layer. There is a shift of 90 mV in the OCP value in the more positive direction, indicating the probability of formation of a more protective surface film.

Table 6 contains the mass-loss-based proportional corrosion rate index values of Al97-Zn3 alloy with and without SiC particulation, as a function of electrolyte pH, inhibitor and temperature. It is clearly seen that SiC particulation of the Al97-Zn3 alloy reveals a drastic lowering of the proportional mass-loss index values in inhibited media at 25, 60 and 100 °C, for both the

Table 4 Hardness (BHN) and I_{corr} (mA/cm^2) values of Cu70-Mn30 composite alloys, as a function of the type of reinforcements (particulate = ultrafine)

Matrix	Hardness (BHN)	I_{corr} (mA/cm^2) (electrolyte = 3% NaCl)
Cu-Mn	69	0.900
Cu-Mn + 1.0% SiC	97	0.420
Cu-Mn + 1.0% Al_2O_3	89	0.0072
Cu-Mn + 1.0% TiO_2	79	0.0074

neutral pH and low pH environments. Looking at these values horizontally, it is further clear that both the temperature and the neutral pH reduce the mass-loss indices, for both the unreinforced and reinforced matrices. It appears that an increase in temperature results in the formation of Al_2O_3 within the inhibited barrier layer, resulting in the drastic lowering of the proportional mass-loss index.

Table 7 lists the physico chemical properties of the Pb composite alloys, as a function of the type of reinforcement. It is clear from this table that reinforcement of the lead matrix with particulates like steel powder and glass powder, which do not fall in the ultrafine category, improves only the dry corrosion resistance ratings, while the proportional mass-loss and OCP values remain more or less unchanged. However, the surface hardness values reveal considerable improvement as a result of matrix reinforcement. All these data clearly indicate that the matrix behaves as a conventional composite matrix, where the reinforcements merely act as stress-raiser sites, increasing the matrix hardness.

Table 8 gives the electrochemical properties of polyaniline matrices with and without fine and coarse fractions of metallic glass (MG), along with the cladding of Pb-Sn and Pb-Sn-MG (finer) composite alloys. Looking at the data vertically, it is clear that reinforcement with MG in the polyaniline matrix reduces the proportional mass-loss indices, irrespective of the type of cladding materials used. The effect is more pronounced in the finer fraction of the MG-reinforced matrix. It is also observed that cladding of pure polyaniline with Pb-Sn alloy makes it more active electrochemically than with the Pb-Sn-MG composite. In all these cases the reduction of mass-loss indices is attributed to the inherent metastability of the MG reinforcements, which tend to undergo instantaneous passivation forming an adherent layer of protective barrier. The MG reinforcements are

Table 3 De-alloying experiment for the Cu60-Zn40-SiC composite alloy [mixed electrolyte = 3% NaCl: 0.5% $NaNO_2$: 0.5% Na_2SO_4 (1:1:1); particulate = ultrafine]

Matrix	De-alloyed component (μg/100 cm^3)					
	Copper			Zinc		
	4 days	6 days	8 days	4 days	6 days	8 days
Cu-Zn	75	20	40	90	90	90
CuZn + 0.20% SiC	91	25	50	112	112	112
CuZn + 0.30% SiC	11	11	14	40	50	60
CuZn + 0.40% SiC	85	30	54	90	90	90

Table 5 Thickness and electrochemical properties of cerium deoxidized Zn97-Al3 coated MS substrate, with and without SiC particulation (electrolyte = 3% Nacl; particulate = ultrafine)

Matrix	Massloss (g/cm²/day)	OCP (mV)	Thickness of coating (µm)
Zn + 3% Al + 1% *misch metal[a]	0.56×10^{-5}	−840	180
Zn + 3% Al + 1% *misch metal + 1.5% SiC	0.22×10^{-5}	−750	190

[a] Misch metal containing 70% Ce, 28% Fe and 2% other rare-earth elements

Table 6 Mass-loss based proportional corrosion rate index values for Al97-Zn3 alloy, with and without particulation, as a function of electrolyte ph, inhibitor and temperature (particulate = ultrafine)

Matrix	Proportional mass-loss index (inhibited with 1% hexamine and 0.1% sodium chromate)					
	25 °C		60 °C		100 °C	
	Low pH	Neutral pH	Low pH	Neutral pH	Low pH	Neutral pH
Al97-Zn3	12.7	2.1	5.9	1.3	3.2	1.2
Al96-Zn3-SiC1	3.4	1.2	1.4	1.1	1.3	1.0

Table 7 Physicochemical properties of Pb composite alloys, as a function of the type of reinforcement (electrolyte = 3% NaCl; particulate = 800 mesh size)

Matrix	Hardness (BHN)	Proportional mass-loss index	OCP (mV)	Porportional oxidation rate index	Potential of the oxidized specimen (mV)
Pure lead	190	1.0	−560	4	−550
Pb + 0.5% steel powder	232	1.0	−530	1	−520
Pb + 0.5% glass powder	250	1.0	−500	3	−480

Table 8 Electrochemical properties of polyaniline (PA) matrices with and without coarse and fine fractions of metallic glass (MG) reinforcement, along with cladding of Pb-Sn and Pb-Sn-MG (fine) composite alloy (electrolyte = 3% NaCl)

Matrix	Proportional mass-loss index	
	Cladding material Pb-Sn	Cladding material Pb-Sn-MG (fine)
Pure polyaniline (PA)	5.3	4.3
Coarse fraction; MG-reinforced PA	4.0	1.70
Fine fraction; MG-reinforced PA	1.0	1.20

within the 0.01–0.1 mm diameter range, being more or less uniformly dispersed within the matrix, and form stress-free zones after the passivation process, reinforcing and enclosing the interaction products from the polyaniline substrate formed at the particulated matrix and electrolyte interface and did not undergo premature spalling during exposure studies.

Table 9 shows the correlation of the ultrafine ceramic particulates and the grain-boundary structures in Zn-Al composite alloys, particulated with 1.5% SiC and 1.5%

Al_2O_3, both belonging to the ultrafine variety. It is seen that the total volume of grains, volume equivalent of total grain-boundary areas and the volume equivalent of other defects are more or less the same for both of these systems, although the latter (Al_2O_3 reinforced matrix) reveals lower I_{corr} values than the former. The Al_2O_3 reinforced matrix also reveals higher values of particulate trapping capacity (PTC) and also higher 'residual PTC', indicating a direct relationship between the trapping of anodic sites by ultrafine partciulates and the dissolution of the matrices. The PTC indicates the total volume of anodic sites such as grain boundaries, voids, vacancies, etc., which can accommodate the ultrafine particulates. The comparatively lower value of 'volume eqauivalent of total particulates' compared to its PTC for the Al_2O_3 reinforced matrix appears to increase the probability of less particulates on the grain proper and more within the anodic sites. As such, the anodic sites are deactivated without creating any extra stress raiser points on the grain proper.

Table 10 lists the I_{corr} values of the ultrafine particulate reinforced matrices as a function of the PTC and the 'galvanic stress factor' (GSF) for Zn-Al

Table 9 Correlation of the ultrafine ceramic particulates and the grain-boundary structures in Zn-Al composite alloys

Matrix	Total volume of grains (cm³)	Volume equivalent of total grain boundary area (cm³)	Volume equivalent of other defects (cm³)	Volume equivalent of other particulates (cm³)	Particulate trapping capacity	Residual particulate trapping capacity of the matrix (cm³)	I_{corr} (µA/cm²)
Zn95.5-Al3-SiC1.5	0.693	0.032	0.275	0.1340	0.307	+0.1730	0.24
Zn95.5-Al3-Al₂O₃1.5	0.617	0.029	0.354	0.0911	0.383	+0.2919	0.12

Table 10 Extrapolated I_{corr} values of the ultrafine particulate reinforced matrices, as a function of the particulate trapping capacity (PTC) and galvanic stress factor (GSF) for Zn-Al matrices containing SiC and Al$_2$O$_3$ particulates in a low concentration range

I_{corr} (μA/cm^2)	PTC of the matrix	GSF of the matrix
0.005	0.45	0.011
0.25	0.30	0.83
0.50	0.15	3.83
0.75	0.01	75.0

matrices containing ultrafine SiC and Al$_2$O$_3$ particulates in a low concentration range. The GSF indicates the stress-raiser activated dissolution of the grain proper, when the ultrafine particulates in excess of the PTC are randomly dispersed within the grain proper. The higher the PTC of a matrix, the lower will be its GSF for a low concentration reinforcement (1–2 wt%) of the matrix by ultrafine particulates. It is seen that the extrapolated values of I_{corr} are directly related to the GSF values and are reciprocally connected to the PTC values. It clearly indicates that lowering of the PTC of a matrix increases the I_{corr} values, as a result of the increase of the GSF.

Table 11 gives the extrapolated mathematical correlation of the I_{corr} (mA/cm^2) values with the PTC and GSF of the Al-Zn alloy matrix, particulated with ultrafine SiC and Al$_2$O$_3$ in a low concentration range. It is clear from these extrapolated correlations that I_{corr} values may be expressed as a mathematical function of the PTC and GSF, within certain specific ranges. A careful observation of the PTC values and their corresponding GSF counterparts clearly corroborates their reciprocal relationship.

Tables 12, 13 and 14 respectively indicate the practical applications of the particulation technique in the enhancement of the corrosion-resistance properties of tin coating for food packaging, an amorphous metal-metalloid Ni-P-B coating for corrosion resistance and a Ni-Fe-Mo type barrier layer on cold-worked copper substrates. It is seen that, for both 6% acetic acid and 6% citric acid media, Sn + 1% SiC surface layer and Sn + 1% SiC bulk alloy reveal lower I_{corr} values and higher B_a values, indicating an anodically activated surface film of a protective nature. It indicates that low concentration particulation of tin with ultrafine SiC may be suitably tailor-made for food packaging in pickle environments, where citric and acetic acids are very common. A similar type of trend is observed in the

Table 11 Extrapolated mathematical correlation of I_{corr} (μA/cm^2) with PTC and GSF for the Al-Zn alloy matrix, particulated with ultrafine SiC and Al$_2$O$_3$ in a low concentration range (1% surface average)

Correlated function	PTC range	GSF range
PTC × GSF = I_{corr}	0.30–0.45	0.011–0.83
PTC × GSF = I_{corr}	0.15–0.30	0.83 –3.33

particulated Ni-P-B type barrier layer, both via electroless and current-assisted electroless routes. Mass-loss values reveal a drastic reduction due to particulation with Al$_2$O$_3$, SiC, BC, WC, etc., particulates. Reduction appears to be more for the current-assisted deposition. These barriers may be potential candidates where both resistance to corrosion and abrasion are the requisites. Permalloys are potential candidate materials for transformer cores and other electrical appliances, where low core-loss is the major criterion. It is seen that particulation in the range of 0.1% enhances the polarization resistance value to a maximum, indicating superior resistance to deterioration and enhancing resistance to surface core-loss in the form of eddy currents.

Tables 15, 16 and 17 list particulation of paint barrier layers, along with X-ray diffraction analysis of the painted panels. Particulation of paint barrier layers of epoxy class in a neutral chloride medium with and without bath oscillation (stirring) appears to improve the resistance to surface deterioration of the paint barrier layers. The OCP values tend to a more positive direction and the galvanic current values indicate a considerable reduction, both at room temperature and at 80 °C (Table 16). Table 17 gives X-ray crystallographic data for the expoxy-based paints, incorporated with ultrafine SiC, coated on low alloy-steel substrates, after exposure in a synthetic seawater bath and stirred at an elevated temperature of 80 °C. It is clearly observed that SiC-reinforced paint layers reveal a 'SiC' signal only after exposure in an elevated temperature, stirred, synthetic seawater bath, indicating that these ultraparticles tend to enter the lower layers which are only revealed after the top layer is dissolved in the stirred bath. The number of peaks revealed by the SiC particulated layer appears to be marginally higher than that without any particulates.

Figure 1 shows the correlation of the mass-loss values of the Zn-SiC composite alloys in the as-cast, stress-relieved and water-quenched states, as a function of SiC concentration. It is seen that the mass-loss values undergo a drastic reduction at around 0.25% SiC concentration. However, the reduction is a maximum in the case of the water-quenched panel, followed by that of the stress-relieved and as-cast ones. Mass-loss values tend to increase at SiC concentrations above 0.25% owing to the dispersion of the particulates within the grain proper. Such dispersion appears to be minimum for the water-quenched panel, followed by that of stress-relieved and as-cast ones. Water quenching of the matrix may be connected to an effective increase of total grain-boundary areas (due to grain refinement) which are the major anodic sites, taking up a large part of the particulates within the grain channels such that very little is left for dispersion within the grain proper.

Figure 2 displays the correlation of I_{corr} values as a function of conventional coarse Al$_2$O$_3$ particulates, reinforced in an electroplated zinc barrier layer, obtained from an acid zinc chloride bath, under potentiostatic control. It is seen that the I_{corr} values reveal a marginally

Table 12 Tafel parameters of coated and bulk samples of Sn, with and without SiC reinforcement

Matrix	6% Acetic acid			6% Citric acid		
	B_a (mV/decade)	B_c (mV/decade)	I_{corr} (mA/cm^2)	B_a (mV/decade)	B_c (mV/decade)	I_{corr} (mA/cm^2)
Sn coating on mild steel	41	25	4.5	44	23	3.5
Sn + 1% SiC coating on mild steel	46	25	3.5	62	24	2.5
Sn + 1% Al$_2$O$_3$ coating on mild steel	39	26	4.5	40	19	6.5
Sn bulk alloy	42	28	2.5	34	21	2.5
Sn + 1% SiC bulk alloy	52	28	1.5	38	21	1.5
Sn + 1% Al$_2$O$_3$ bulk alloy	30	23	2.5	36	24	5.5

Table 13 Physicochemical properties of an amorphous Ni-P-B[a] coated mild steel substrate, with and without co-deposition of ceramic particulates

Matrix	Current-assisted electroless			Electroless		
	Average hardness (VPN)	Average thickness (μm)	Mass-loss value (mdd) (3% naCl)	Average hardness (VPN)	Average thickness (μm)	Mass-loss value (mdd) (3% NaCl)
Amorphus Ni-P-B (no particulates)	1200	40	1.33	–	–	–
Amorphous Ni-P-B + 5SiC-5WC-1.5Al$_2$O$_3$	1400	32	0.22	–	–	–
Amorphous Ni-P-B + 5SiC-5WC-1.5Al$_2$O$_3$	–	–	–	1400	13	0.39
Amorphous Ni-P-B + 5SiC-5WC-5BC-5Al$_2$O$_3$	–	–	–	1400	11	0.57

[a] Ni-P-B = nickel phosphorus boron electrodeposited on mild steel, using a current-assisted electroless bath

Table 14 Electrochemical properties of the Ni-Fe-Mo type permalloy coating, after contamination of the bath with different Al$_2$O$_3$ concentrations

%Al$_2$O$_3$ in the citrate-based permalloy bath	Ratio of metallic (a) to particulate (b) coverage = a/b ($\times 10^{-3}$)	Polarization resistance Rp (ohms)	Potential (mV) vs. SCE (3% NaCl)		
			Initial	After 10 days	After 20 days
0	1	683	−251	−200	−60
0.1	9	1083	−225	−100	−10
0.2	18	966	−230	−180	−50
0.3	28	883	−240	−200	−50
0.5	51	741	−260	−200	−50

Table 15 Physical and chemical properties of epoxy-painted low alloy steel (LAS) with and without SiC particulation, exposed in neutral medium

Panels and media	Potential (mV)		Hardness (BHN)		Observation
	Initial	After 30 days	Initial	After 30 days	
Medium = 3% NaCl, zinc epoxy (100 μm) + 180 μm epoxy-silicone topcoat	−5.0	−84.0	40	45	Slight staining
Medium = 3% NaCl, zinc epoxy (100 μm) + 180 μm epoxy-silicone topcoat (1% SiC)	−5.0	−50.0	50	55	No pitting or staining
Medium = tap water, zinc epoxy (100 μm) + 180 μm epoxy-silicone topcoat	−4.0	−22.0	50	55	Slight staining
Medium = tap water, zinc epoxy (100 μm) + 180 μm epoxy-silicone top-coat (1% SiC)	−4.0	−10.0	60	65	No pitting or staining

decreasing trend with an increase in Al$_2$O$_3$ concentration. The marginal reduction may be attributed to the presence of some ultrafine particulates and dusty particles present as an impurity, such that the comparatively coarser Al$_2$O$_3$ particles make an unsuccessful attempt at covering the anodic areas and mostly generate stress spikes, simultaneously with the coverage obtained, if any.

Figure 3 reveals the correlation of Cu60-Zn40-BC composite alloys, in the as-cast, stress-relieved and water quenched states, as a function of % BC. It is seen that the mass-loss values tend to a minimum at around 0.25% BC concentration, followed by a drastic increase above that concentration as a result of the dispersion of the BC particulates within the grain proper. However, as in the case of Zn-SiC particulation, water quenching

Table 16 Galvanic current scanning of epoxy-based coating on LAS substrate with and without SiC particulation obtained in a stirring condition both at room temperature and at elevated temperature (medium = synthetic sea water; temp. 30–80 °C; stirring speed = 3000 r.p.m.)

Panels	Current (mA)			
	Initial		After 7 days	
	30 °C	80 °C	30 °C	80 °C
60 µm epoxy-silicone primer + 60 µm epoxy-silicone topcoat	200	200	200	200
60 µm epoxy-silicone primer + 60 µm epoxy-silicone topcoat (1% Sic)	150	60.5	150	150
100 µm epoxy-silicone primer + 100 µm epoxy-silicone topcoat (1% SiC)	150	68.5	160	170

Table 17 X-ray crystallographic data for epoxy-based paints, incorporated with ultrafine SiC and coated on LAS after exposure in a synthetic seawater bath stirred at elevated temperature (bath temp. = 80 °C; stirring speed = 3000 r.p.m.; 'd' value of α-SiC = 2.54–2.56)

Paint barrier layer	Reinforcement of paints and exposure of panels	No. of peaks in X-ray plot	'2θ' equal to near that of 'α-SiC'	Corresponding 'd' values	Conclusion
60 µm epoxy-silicone primer + 60 µm silicone topcoat	'SiC' reinforcement in top layer and not exposed in electrolyte	16	36.6 33.7	2.453 2.657	No 'SiC' in top layer
60 µm epoxy-silicone primer + 60 µm silicone topcoat	'SiC' reinforcement in top layer and exposed in electrolyte	18	35.0 36.3 33.7	2.562 2.590 2.657	'SiC' signal available in top layer

revealed lower mass-loss values, probably due to the lower particulate dispersion within the grain proper.

Figure 4 shows the effect of thermomechanical treatment (TMT) on the corrosion behaviour of a Cu60-Zn40-SiC composite alloy matrix as a function of SiC concentration. It is clearly seen that for both the as-cast and thermomechanically treated panels the mass-loss values tend to a minimum and the potential values tend to a more positive direction at around 0.25% SiC concentration. It appears further that application of the TMT has brought down the mass-loss values to a considerable extent and has also caused considerable positive shifts in the level of the potential values. TMT appears to have increased the total anodic sites of the matrix, for the

habitation of the ultrafine particulates, such that there is an effective decrease in the extent of particulates available for dispersion within the grain proper.

Figure 5 reveals the effect of TMT on the mass-loss values for the ultrafine BC particulated Cu60-Zn40 matrix. As in the case of SiC particulation, these matrices also reveal a polarization at around 0.25% BC, for the electrochemical potential and mass-loss data, both of which tend to decline at that point. The level of mass-loss values also reveals a considerable reduction as a result of TMT.

Figure 6 shows the correlation of surface hardness and I_{corr} values of the Cu60-Zn40-SiC composite alloys with the SiC concentration of the matrix. It is seen that the hardness values reveal a more or less increasing trend as a result of particulation, for both the as-cast and the
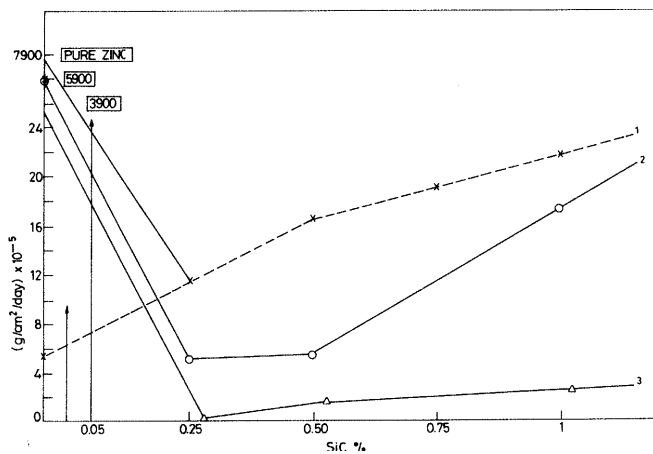

Fig. 1 Correlation of mass-loss values for Zn-SiC composite alloys in the as-cast (X), stress-relieved (○) and water-quenched (△) states, as a function of SiC concentration
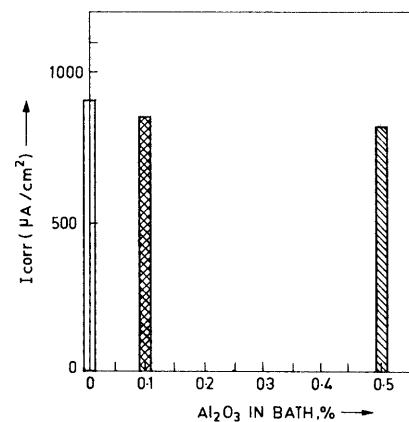

Fig. 2 I_{corr} values as a function of the conventional Al_2O_3 particulates in electro-deposited zinc
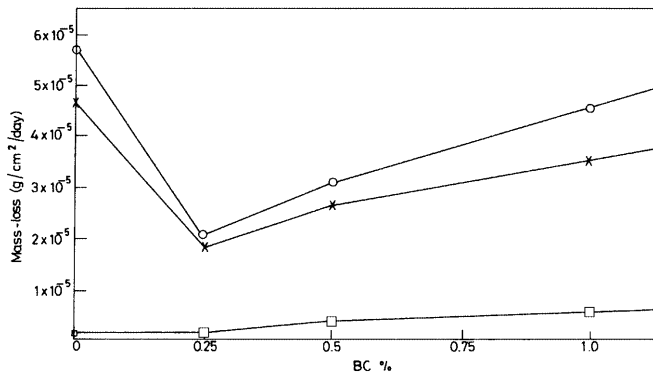
Fig. 3 Mass-loss values of Cu60-Zn40-Bc composite alloys, in the as-cast (○), stress-relieved (X) and water-quenched (□) states
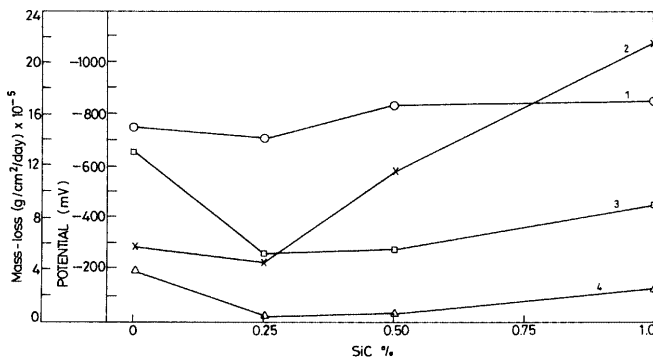

Fig. 4 Effect of thermomechanical treatment (TMT) on the corrosion behaviour of Cu60-Zn40-SiC composite alloy, as a function of SiC-concentration: X as-cast (mass loss); ○ as-cast (potential); △ TMT (mass loss); □ TMT (potential)
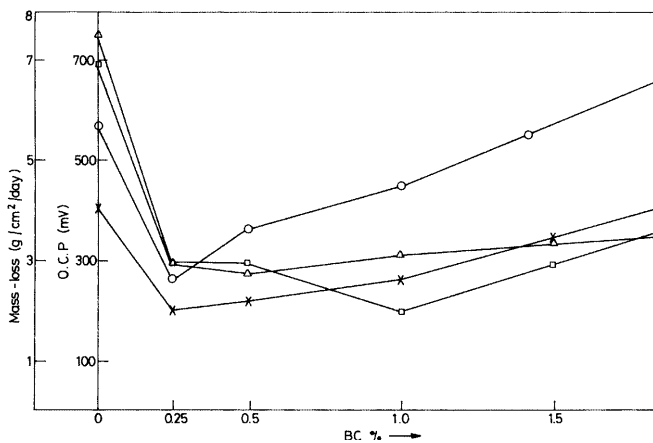

Fig. 5 Effect of TMT on the ultrafine BC particulated Cu60-Zn40 Brass: ○ as-cast (mass loss); △ as-cast (potential); X TMT (mass loss); □ TMT (potential)

Fig. 6 Correlation of surface hardness and I_{corr} values of Cu60-Zn40-SiC composite alloy, as a function of SiC concentration (%): X as-cast (hardness); ○ homogenized (hardness); as-cast (I_{corr}); □ homogenized (I_{corr})
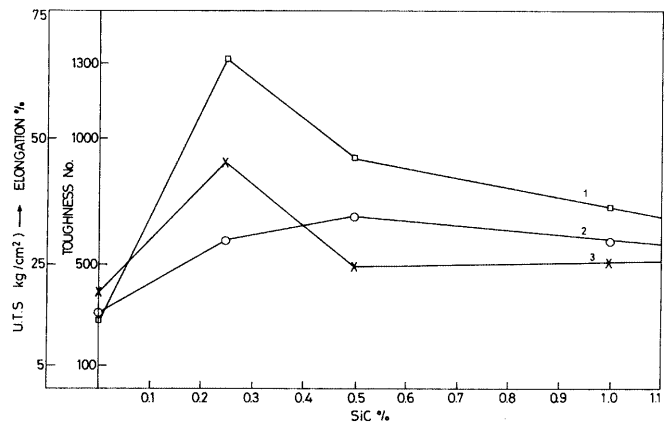
Fig. 7 Mechanical properties of Cu60-Zn40-SiC composite alloys as a function of %SiC: ○ UTS; X %elongation; □ toughness

Figure 7 displays the correlation of mechanical properties of Cu60-Zn40-SiC composite alloys with the SiC concentration of the matrix. It is clearly observed that the mechanical properties attain a peak value within a particulation range of 0.25–0.5% SiC, followed by a progressive decline. Such mechanical behaviour corroborates the criticality of the 0.25–0.50% particulation range, indicating a probable compatibility in both the electrochemical and mechanical behaviour of the matrix.

Figure 8 reveals the correlation of mass-loss values of the Cu60-Zn40-SiC alloy with the SiC concentration of the matrix, in the presence and absence of magnetic fluxes in a low pH chloride-containing medium. It is seen that the mass-loss values tend to a minimum at around 0.25% SiC concentration, followed by an increase above that point. However, a considerable increase in the level of mass-loss values is observed as a result of application of the magnetic flux from an external source, compared to the panels where no magnetic flux is employed. This is
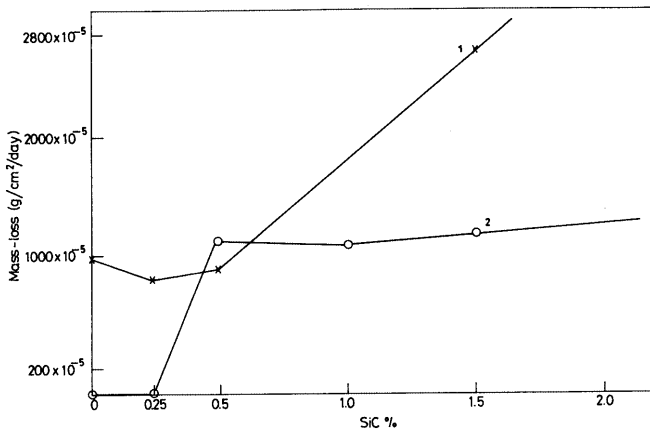
homogenized matrices, while the I_{corr} values tend to increase beyond 0.25–0.5% SiC concentration, indicating the presence of a threshold level of anodic defects, available on the matrix, for subsequent particulate trapping.

Fig. 8 Correlation of mass-loss values of a Cu60-Zn40-SiC matrix with SiC concentration, in presence and absence of magnetic flux: ○ without magnetic flux; X with magnetic-flux

attributed to the accelerated surface dissolution, induced by the magnetohydrodynamic forces due to the interactions of the surface double-layer capacitance and galvanic forces with those of the applied magnetic flux.

Figures 9 and 10 depict the correlation of mass-loss and I_{corr} values of CuZn, Zn-Al-Ce and CuMn alloys, etc., with their ultrafine matrix reinforcements. It is seen that the mass-loss (mdd) values of the unparticulated Cu-Zn matrix increase in the order quenched, TMT, stress-relieved (heated in air environment) and as-cast, while this order changes to quenched, stress-relieved in air environment, TMT and as-cast after particulation of the matrix with BC. It is clearly observed that particulation brings down the level of mass loss to a considerable extent, in all the above states. In the process there is an exchange of place between TMT and stress-relieved panels. It also indicates that the as-cast panel reveals the maximum mass loss, while particulated and quenched panels reveal the minimum. Comparing the panels of
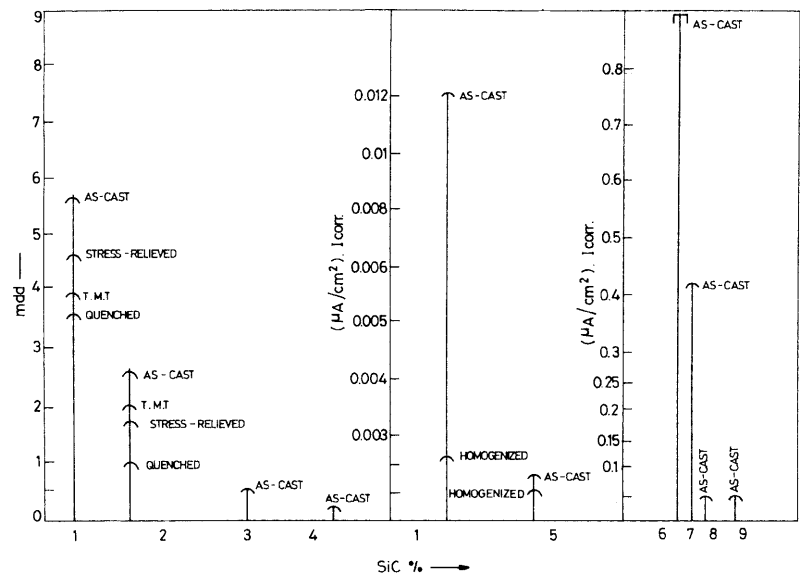
Zn-Al-Ce and Zn-Al-Ce-SiC, it is observed that particulation causes an almost 50% reduction of mass-loss value of the Zn-Al-Ce (misch metal) matrix. It is also observed that the particulation of the pure Cu-Zn matrix with SiC causes a considerable reduction of the level of I_{corr} values, in both the as-cast and homogenized state. Nevertheless, the homogenized panel reveals lower mass-loss values in both the unparticulated and particulated states. It is further observed that particulation of the Cu-Mn matrix causes a considerable decrease of the mass-loss values, particularly with 1% Al_2O_3 and 1% TiO_2 particulates, where a reduction as high as 88% is achieved.

Figure 11 depicts the comparison of the volume equivalent of grain-boundary structures and micro-voids, etc., and of particulates and particulate trapping capacity, for the matrices 95.5Zn-3Al-1.5SiC and 95.5Zn-3Al-1.5Al$_2$O$_3$. It is observed that in the case of the latter with ultrafine Al_2O_3 as the reinforcement, the volume equivalent of micro-voids, etc., is more but the volume equivalent of the particulates is less than that of the former matrix, where ultrafine SiC has been used for reinforcement. Accordingly, the latter matrix has higher particulate trapping capacity than the former, as the total available anodic sites for accommodating particulates is more in this case compared to the volume equivalent of the particulates, such that the probability of particulates being dispersed within the grain proper becomes a minimum. As such, the matrix reveals lower surface dissolution in terms of I_{corr}.

Figure 12 shows the electrochemical properties of coated and bulk tin, as a function of SiC and Al_2O_3 concentration, in 6% citric acid. It is clearly observed that particulation of the tin matrix with SiC particulates, which are of the ultrafine variety, results in lowering of matrix I_{corr} values for both the tin coating and the bulk tin coating. On the other hand, particulation of the tin matrix with the conventional Al_2O_3 particulates (250

Fig. 9 Correlation of mass-loss values, with ultrafine particulation of CuZn alloys: 1 Cu60-Z40; 2 Cu60-Zn39.75-BC0.25; 3 Zn96-Al3-Ce1; 4 Zn95.5-Al3-SiC1.5
Fig. 10 Correlation of I_{corr} values with ultrafine partciulation of CuZn alloys: 1 Cu60-Zn40; 5 Cu60-Zn39.75-SiC0.25; 6 Cu70-Mn30; 7 Cu70-Mn39-SiC1; 8 Cu70-Mn39-Al$_2$O$_3$1; 9 Cu70-Mn39-TiO$_2$1

Fig. 13 Electrochemical properties of coated and bulk tin as a function of SiC concentration, in 6% acetic acid solution: ○ Sic; X Al_2O_3
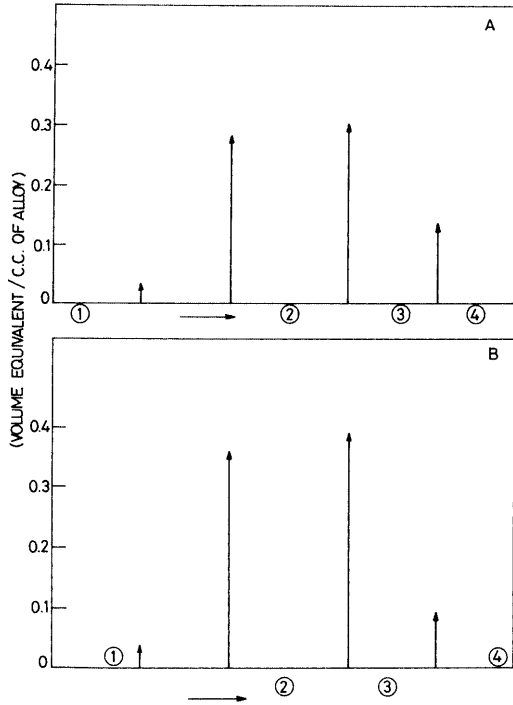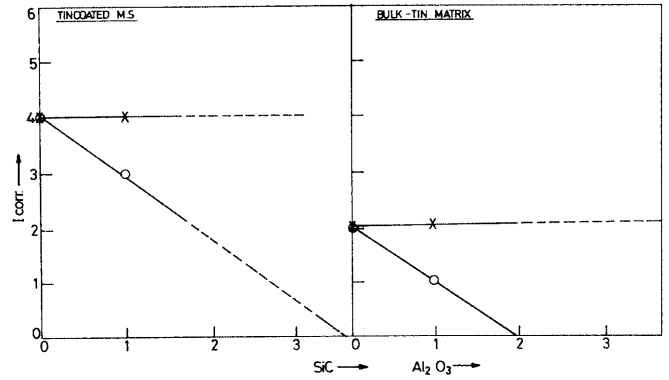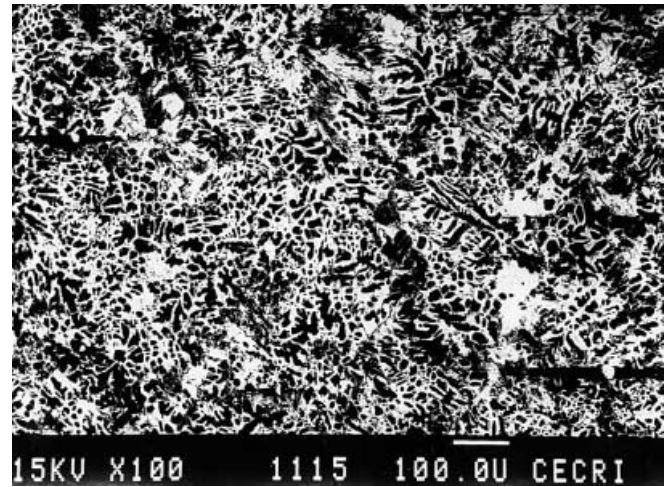
Fig. 11 Volume equivalent of grain boundary structure, particulates and particulate trapping capacity. *Top*: Zn95.5-Al3-SiC1.5 (I_{corr} = 0.24 μA/cm^2). *Bottom*: Zn95.5-Al3-Al$_2$O$_3$1.5 (I_{corr} = 0.12 μA/cm^2). 1 Volume equivalent of grain boundaries; 2 volume equivalent of micro-voids and other defects; 3 particulate trapping capacity; 4 volume equivalent of particulates

Fig. 14 SEM micrograph of Zn-BC matrix
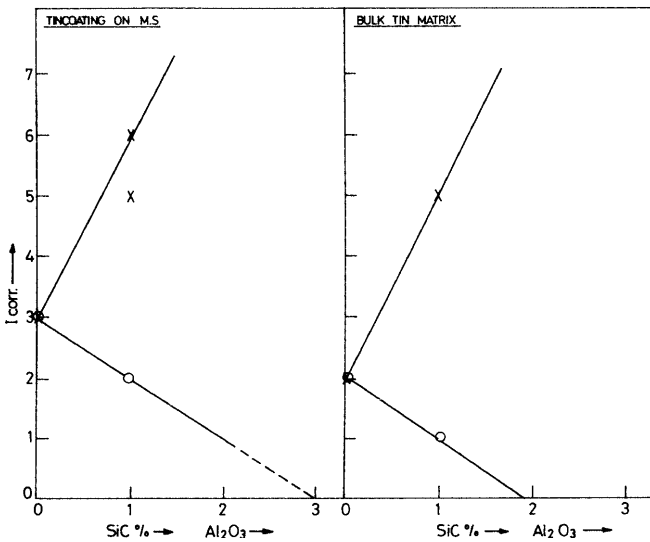
Fig. 12 Electrochemical properties of coated and bulk tin as a function of SiC concentration, in 6% citric acid: ○ SiC; X Al$_2$O$_3$

with increase in the concentration of ultrafine SiC in the matrix with 2–3 wt% in both the coating and the bulk matrix, while increase in the concentration of the conventional coarse alumina powder, within that range, remains ineffective in reducing I_{corr} values.

Figure 14 depicts the SEM structure of a 1% BC particulated zinc matrix, while Figs. 15 and 16 show the optical micrographs of 1% Al$_2$O$_3$ and 1% SiC particulated zinc matrices. It is clearly seen that the particulates arrange themselves in a more or less network pattern on the matrix. Network formation is more prominent in the Zn-SiC matrix than in those of the Zn-BC and Zn-Al$_2$O$_3$ matrices. Figure 17 displays the network formation of the SiC particulates on a Zn95.5-Al3-SiC1.5 matrix. These unique surface patterns corroborate the assumption that ultrafine particulates are preferentially organized along the anodic grain boundaries and other defect sites. Figure 15, in revealing the Zn-Al$_2$O$_3$ matrix, clearly indicates the coverage of particulates along the grain boundaries. Figures 18 and 19 respectively show uncorroded tin-coated MS with and without SiC
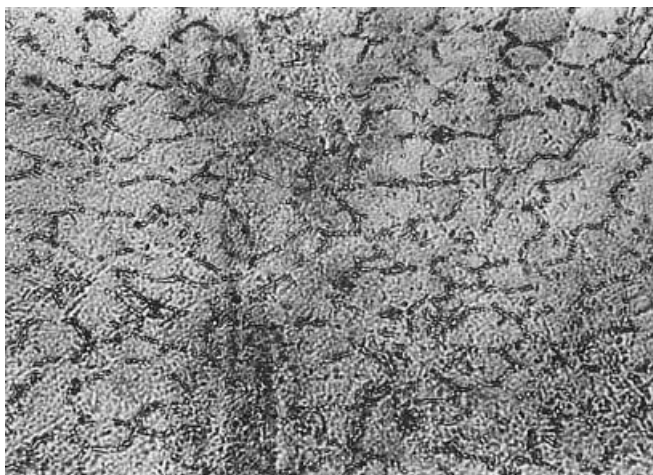
mesh size) takes the I_{corr} values along the upward direction for both the coating and the bulk matrix.

Figure 13 reveals the electrochemical properties of the coated and bulk tin as a function of SiC and Al$_2$O$_3$ concentration in 6% acetic acid solution. In this case, the I_{corr} values reveal a progressively decreasing trend

Fig. 15 Optical micrograph of Zn-Al$_2$O$_3$ matrix

Fig. 17 SEM micrograph of Zn95.5-Al3-SiC1.5 matrix

Fig. 16 Optical micrograph of Zn-SiC matrix

Fig. 18 Optical micrograph of uncorroded Sn-coated MS, without SiC particulation
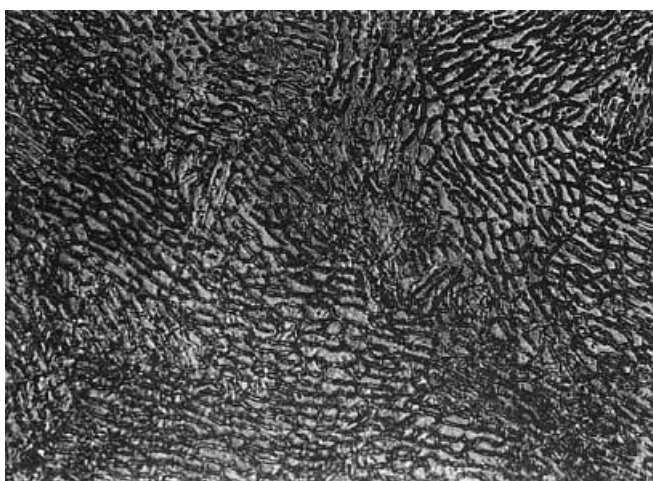

Fig. 19 Optical micrograph of uncorroded Sn-coated MS, with SiC particulation

particulates, while Figs. 20 and 21 display those of their corroded counterparts. SiC particulates are clearly observed, distributed more or less uniformly, in both the uncorroded and corroded Sn-coated MS substrates.

Summary and conclusions

Looking at the data presented in Tables 1–11 and Figs. 1–21, it is clear that particulation with ultrafine SiC particulates in a low concentration range (1–2 wt%) improves the resistance to surface dissolution of matrices like pure zinc, Cu60-Zn40, Cu70-Mn30, Zn96-Al3-Ce(misch metal)1, Al97-Zn3-Ce(misch metal)1 and pure tin. It has also been observed that ultrafine particulates like BC, WC, Al$_2$O$_3$, etc., behave in a more or less similar manner to SiC. It appears that ultrafine ceramic particulates in a low concentration range sit and cover the anodic matrix sites like grain boundaries, micro-voids, etc., and thereby reduce the total anodic current
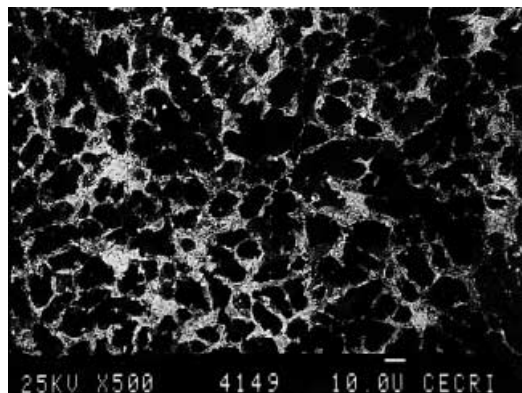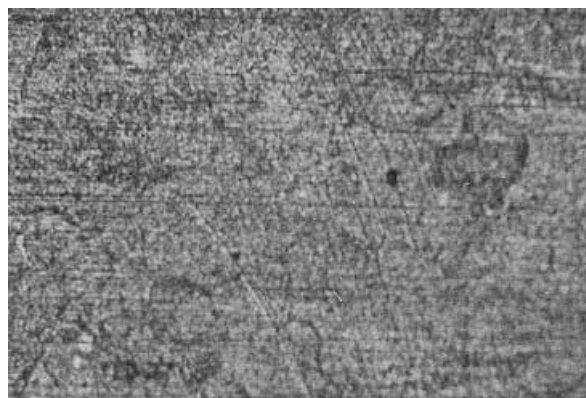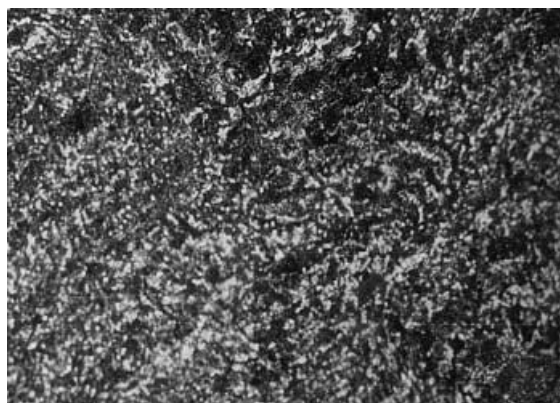
of the matrix. The tendency of the ultrafine particulates to be arranged around grain and subgrain boundaries is clearly revealed from photomicorgraphic studies for these alloys. Photopotential measurements on Cu60-Zn40 alloy, particulated with ultrafine SiC, BC or WC in 0.5 M NaOH medium, also corroborated such an inference. De-alloying studies on Cu60-Zn40 alloy
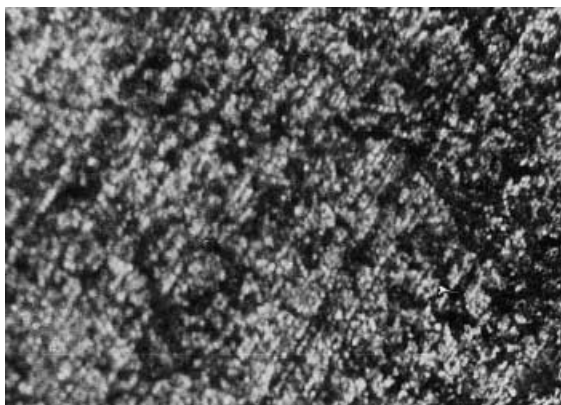
Fig. 20 Optical micrograph of corroded Sn-coated MS, with SiC particulation
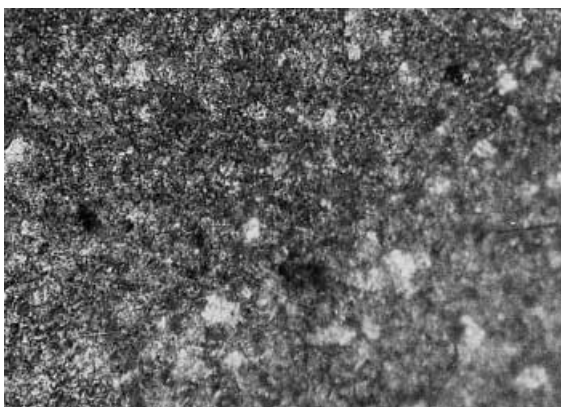

Fig. 21 Optical micrograph of corroded Sn-coated MS, with SiC particulation

particulated with ultrafine SiC revealed that there is suppression of both Cu and Zn de-alloying processes, within a particulate concentration range of 0.2–0.4%. It is assumed that a particular metallic matrix has a quantified number of available anodic sites, such that it can accommodate a critical amount of ultrafine particules within these sites, depending on the total volume equivalent of the matrix anodic sites and those of the particulates. However, the particulates in excess of the matrix capability are dispersed within the grain proper, creating stress-raiser sites and subsequent enhanced galvanic interaction. From the collected experimental data, such critical particulation appears to lie at or near 0.25% concentration for the pure zinc and Cu60-Zn40 matrices with ultrafine particulates like SiC and BC.

TMT, quenching and stress relief appear to further improve the resistance to surface dissolution of these matrices. Such improvements have been connected to processes like grain refinement, generation of newer grain-boundary areas, and vacancies and matrix re-crystallization, creating excess sites for the trapping of ultrafine particulates. In the case of Zn-Al-Ce (misch metal) and Al-Zn-Ce (misch metal) systems, SiC

particulation has resulted in the improvement of resistance to matrix leaching in both the uninhibited and inhibited media, in both neutral and low pH environments at room temperature and elevated temperatures. It further appears that low concentration particulation of the popular binary and tertiary alloys not only de-activates the electrochemical interactions on the surface, but also improves the mechanical properties like hardness, UTS, elongation and toughness of the matrix, depending on the chemistry and metallurgy of the matrix and the reinforcement. It has been observed that incorporation of low concentrations of ultrafine SiC in conventional tin coatings improves its resistance to dissolution in media like 6% acetic acid and 6% citric acid. It indicates the possibility of exploitation of this particulated class of tin coating for the packing industry. Use of conventional coarse-steel powders and glass powders which are not of the ultrafine variety may eventually improve the oxidation resistance and hardness of the conventional lead lining, without improving the resistance to surface dissolution, both at room temperature and at elevated temperatures. The same thing applies to the particulation of the tin barrier and electroplated zinc layer with conventional coarse Al_2O_3 powders, where corrosion resistance properties are either degraded or only marginally improved. Corrosion resistance of zinc and its alloys, which find extensive industrial applications, may be considerably enhanced by such low concentration, ultrafine particulation processes. It appears that dissolution characteristics of the conventional brass surfaces may be tailor-made by keeping the particulate concentration within the threshold critical limit and raising it above that limit for applications requiring respectively resistance to corrosion and enhancement of dissolution. Such innovative design may be of considerable help in reducing the galvanic mismatch in compound-type structures, like stainless steel with brass and carbon steel with brass, by marginally increasing and decreasing the corrosion resistance of the brass surfaces, within the limit of allowable design consideration. Practical applications of this unique technique of low concentration particulation of the metallic matrices may result in considerable economy, considering the massive investments in the field of food packaging industries, amorphous matrices and permalloy-glass materials, for use in transformer cores and paint barrier layers, requiring resistance to corrosion, oxidation and abrasion. The same may be the comment regarding the low concentration particulation of zinc and brass matrices with ultrafine particulates of SiC. This is particularly useful to flatten the galvanic strains, imposed on engineering surfaces, as a result of the complex compound-type designs, where more active steel parts are used in contact with more the cathodic type of brasses. This may attain real significance in the case of strategic applications, where the formation of minutes specks of corrosion products may jeopardize the whole system, as in miniaturized equipment, micro-components and other electronic circuits.

Studies conducted on the correlation of grain boundary structures and other parameters of ultrafine particulation have revealed that for an optimum trapping of matrix anodic sties there should be compatibility between the total volume equivalent of the matrix anodic sites and the total volume equivalent of the reinforcing ultrafine particulates, such that after coverage of the anodic sites there is no reinforcing particulates left within the grain proper to create stress-raiser sites and subsequent enhanced galvanically induced dissolution. From the experimental data collected on the Zn97-Al3 composite alloys, particulated with ultrafine SiC and Al_2O_3 in a low concentration range (1–2 wt%), it is clear that surfaces having a higher PTC reveal lower I_{corr} values and vice versa. However, the PTC of the composite alloy matrix appears to be reciprocally connected to the GSF, such that higher particle trapping is associated with lower galvanic interactions, as very few particulates are available for dispersion on the grain proper. Moreover, PTC may be mathematically connected to the GSF via I_{corr} values of the matrix, such that knowledge of any two of them may provide the third one.

References

1. Balakrishnan K, Venkatesan VK (1978) Werkst Korros 29: 113–122
2. Sato N (1989) Corrosion 45: 354–368
3. Balluci F, Nicodemo L, Bongiovanni A, Martino D, Capobianca G (1987) Galvanic corrosion at composite metallic-material interface. Preprint, 10th international conference on metallic corrosion. Madras, India, vol 1, pp 633–642
4. Chyou SD, Shih HC, Sinchua H (1990) Mater Sci Eng A 129 A
5. Kendig M, Jeanjaqual S, Lumsden J, Hardwick D (1990) Proc Electrochem Soc vol 90, pp 33–40
6. Sokolov YV, Kochan GV (1990) Vestsi Akad Navuk BSSR Ser Tekh Navuk (4): 38–42
7. Mizuki H, Fukumoto HC (1992) Bio Sci Kauri vol 36, pp 122–128
8. Tsubota M, Honda K, Makino Y (1991) Corrosion and wear resistant material for light water nuclear rectors. Jpn Kokai Tokkyo Koho 63: 285–047
9. Grunkel R, Peichl L, Smarsly W, Eichmann W (1993) Ger Pat 4, 222, 210
10. Brown R, Alias MN, Foutana R (1993) Surf Coat Technol 62: 467–473
11. Frangini S, De Christofaro N, Lascovich J, Mignone A (1993) Corros Sci 35: 153–159
12. Vityal P, Verstak A, Talako T, Sobolevsky S, Luigscheider E, Jokel P, Beckschulte G, Yuschenko K, Purusche G (1993) Mater Sci Eng A 168: 61–66
13. Roepsorff S, Maahn E (1992) Corrosion resistance of aluminium-silicon carbide composite materials. In: Tuturi PJ (ed) 2nd corrosion congress (eurocorr). Corrosion society of Finland, Helsinki, pp 279–287
14. Sathyanarayanan S, Manoharan SP, Rajagopal G, Balakrishanan K (1992) Br Corros J 27: 72–74